RSC Advances

PAPER

View Article Online
View Journal | View Issue

Cite this: *RSC Adv.*, 2015, **5**, 52896

Electrocatalytic synthesis of poly(2,6-diaminopyridine) on reduced graphene oxide and its application in glucose sensing

Yong Qin,[a] Jie Yuan,[a] Jianfeng Ma,[a] Yong Kong,*[a] Huaiguo Xue*[b] and Yonggang Peng[c]

Received 23rd April 2015
Accepted 11th June 2015

DOI: 10.1039/c5ra07345f

www.rsc.org/advances

Reduced graphene oxide (RGO) was prepared *via* electrochemical reduction of graphene oxide (GO), and it can effectively catalyze the polymerization of 2,6-diaminopyridine. Poly(2,6-diaminopyridine) (PDAP) deposited on RGO (PDAP-RGO) has good electroactivity in a wide pH range until pH 11.0. Due to the electrocatalytic reduction of H_2O_2 at the PDAP-RGO, a platform for glucose sensing was constructed by immobilizing glucose oxidase (GOD) into the PDAP-RGO. The proposed glucose sensor exhibited a wide linear range from 0.05 to 6.65 mM, a low detection limit of 0.142 μM, a good reproducibility and stability. The apparent Michaelis–Menten constant of GOD was also calculated based on the relationship between steady-state current and glucose concentration.

Introduction

Since the discovery of polyacetylene at the end of the 1970s,[1] conducting polymers (CPs) have attracted increasing attention due to their unique optical, electrical and magnetic properties. Among various monomers suitable for the synthesis of CPs, 2,6-diaminopyridine, the chemical structure of which is similar to *m*-phenylenediamine, is an ideal candidate to be polymerized.[2] In fact, several previous papers on the electrosynthesis of poly(2,6-diaminopyridine) (PDAP) have been reported.[3–5]

Graphene (G), a single layer of sp^2 bonded carbon atoms, has attracted a great deal of attention because of its high electrical conductivity, large specific surface area and excellent mechanical strength.[6–8] Recently, the electrocatalytic polymerization and copolymerization of aniline and its derivatives on reduced graphene oxide (RGO) modified electrode have been reported by Mu *et al.*[9,10] and our group.[11,12] Due to the synergistic effect of CPs and G, numerous work on CPs-G (RGO) based glucose sensors, such as polyaniline-G,[13] polypyrrole-G,[14] and poly(3,4-ethylenedioxythiophene)-G[15] have been reported.

Herein, we investigated the electrocatalytic effect of RGO for the electrosynthesis of PDAP, and the obtained PDAP film deposited on RGO (PDAP-RGO) was characterized by scanning electron microscopy (SEM) and cyclic voltammetry (CV). The as-prepared PDAP-RGO exhibited an improved pH dependence compared with PDAP electrodeposited directly on glassy carbon electrode (PDAP-GCE), *i.e.*, PDAP-RGO has good electroactivity in a wider pH range than PDAP-GCE. More interestingly, the PDAP-RGO showed obvious electrocatalysis towards the reduction of H_2O_2 due to the synergistic effect of RGO and PDAP. And therefore, a sensitive glucose sensing platform was constructed by immobilizing glucose oxidase (GOD) into the PDAP film, and the analytical performances of the novel glucose sensor were also investigated in detail.

Experimental

Reagents and apparatus

2,6-Diaminopyridine and natural graphite powder (99.95%, 8000 mesh) were purchased from Sinopharm Chemical Reagent Co., Ltd. (Shanghai, China). All other chemicals were of analytical grade and used as received. The solutions were prepared with ultrapure water (18.2 MΩ). The human blood serum samples were obtained from Changzhou no. 2 People's Hospital, and the experiments involving them were carried out in line with the institutional guidelines of Changzhou/Yangzhou University and consent was obtained for their use from Changzhou no. 2 People's Hospital. All electrochemical experiments including CV and chronoamperometry were carried out on a CHI 660D electrochemical workstation (Beijing, China). SEM images of different samples were recorded with a model JSM-6360LA scanning electron microscope (Japan). The FT-IR and Raman spectra of GO and PDAP-RGO were recorded on a FTIR-8400S spectrometer (Shimadzu, Japan) and a HR EVOLUTION Raman microscope (Jobin Yvon, France), respectively.

[a]*Jiangsu Key Laboratory of Advanced Catalytic Materials and Technology, School of Petrochemical Engineering, Changzhou University, Changzhou 213164, P. R. China. E-mail: yzkongyong@126.com; chhgxue@yzu.edu.cn*

[b]*School of Chemistry and Chemical Engineering, Yangzhou University, Yangzhou 225002, P. R. China*

[c]*Jiangsu Key Laboratory of Fine Petrochemical Engineering, Changzhou University, Changzhou 213164, P. R. China*

Preparation of RGO modified GCE

Graphene oxide (GO) was prepared from natural graphite powder according to an improved Hummers' method,[16] and the dialysis of GO was carried out for one week to remove the residual acids and salts. GO dispersion was obtained by sonicating 10 mg GO in 10 mL ultrapure water for 90 min, and then 5 μL GO dispersion (1 mg mL^{-1}) was dropped onto the surface of a GCE (3 mm in diameter) and left to dry in ambient air. Finally, the GO modified GCE was electrochemically reduced at −1.0 V for 1 h in 0.1 M N_2 saturated PBS (pH 7.0),[17,18] and RGO modified GCE was obtained.

Electrocatalytic synthesis of PDAP on RGO modified GCE

Electrosynthesis of PDAP-RGO was carried out in a solution of 0.1 M NaOH containing 0.1 M NaH_2PO_4 and 20 mM 2,6-diaminopyridine by CV in a conventional three-electrode cell, which consists of the RGO modified GCE as the working electrode, a platinum foil as the auxiliary electrode and a saturated calomel electrode (SCE) as the reference electrode. The cycling potential was controlled in the range between 0 and 1.4 V at the scan rate of 100 mV s^{-1}, and the electrolysis was finished after 20 cycles. After that, the deposited PDAP film was washed with water to remove unreacted monomers, and then dried in ambient air. For a control experiment, PDAP-GCE was prepared by the same procedure using GCE as the working electrode.

Construction of glucose sensing platform

A volume of 5 μL 1 mg mL^{-1} glucose oxidase (GOD) solution was dropped onto the surface of the as-prepared PDAP film and dried at room temperature. Next, 5 μL of 0.5% Nafion solution was dropped onto the surface of the GOD immobilized PDAP film to maintain the stability of the glucose sensor. The prepared glucose sensor was stored at 4 °C in a refrigerator when not in use. The chronoamperometric responses of glucose at the PDAP-RGO based sensor were recorded at −0.45 V in 0.1 M PBS (pH 7.0) under stirring at room temperature.

Results and discussion

Catalytic polymerization of 2,6-diaminopyridine on RGO

The cyclic voltammograms of the electrochemical polymerization of 2,6-diaminopyridine at bare GCE and RGO modified GCE are shown in Fig. 1. At the bare GCE, an irreversible and broad oxidation peak appears at 0.60 V on the first cycle (Fig. 1A), which is due to the monomer polymerization.[5] It is amazing that two irreversible oxidation peaks with remarkably increased current appear at the RGO modified GCE on the first cycle (Fig. 1B). The peak at 0.45 V is indicative of the formation of radical cations; and the peak at 0.78 V is attributed to the oxidation of monomers. It is clear that RGO plays a significant role in the electrocatalytic synthesis of PDAP. The catalytic effect of RGO may be ascribed to the delocalized π-electrons of G,[19] which lead to the formation of strong π-stacking interactions between RGO and aromatic compounds and their derivatives.[20] The peak currents decrease significantly from the second cycle, suggesting that PDAP film is formed on the RGO modified GCE. Since PDAP belongs to organic semiconductor, and its electrical conductivity is much lower than that of RGO. And therefore, the deposited PDAP on RGO will hinder the further electrodeposition of PDAP film.

Characterization of PDAP-RGO

SEM images of PDAP-GCE and PDAP-RGO are shown in Fig. 2A and B, respectively. It is found that compared with PDAP-GCE, PDAP-RGO exhibits a more compact morphology without obvious embedded cavities, indicating that the existence of RGO is beneficial to the formation of compact and uniform PDAP film.

Fig. 3A shows the FT-IR of GO and PDAP-RGO. For GO, the peaks at 3435, 1737, 1220 and 1058 cm^{-1} are associated with the oxygen-containing groups including –OH, C=O and C–O.[21] These characteristic peaks disappear completely at the PDAP-RGO due to the electrochemical reduction of GO to RGO, and several new peaks at 3330, 3195 and 1421 cm^{-1} corresponding to the stretching vibrations of $–NH_2$ and C–N are observed, which are originated from PDAP. Fig. 3B shows the Raman spectra of GO and PDAP-RGO. It can be seen that the Raman spectra of GO and PDAP-RGO exhibit two prominent peaks of D and G bands at 1349 and 1587 cm^{-1}, respectively. Generally, the intensity ratio of D band to G band (I_D/I_G) is used to estimate the disorder of G.[22] The intensity ratio of PDAP-RGO (1.16) is higher than that of GO (1.02), suggesting that GO is reduced to RGO after the electrochemical treatment.

Fig. 4A shows the cyclic voltammograms of RGO and PDAP-RGO in 0.1 M PBS (pH 7.0). A pair of broad redox peaks (−0.03 and −0.26 V) appears at the RGO, which may be attributed to the subtle incomplete electrochemical reduction of oxygen groups. It is interesting to find that at the PDAP-RGO, the redox peaks appear at nearly identical potentials to those at the RGO, meanwhile the peak currents increase a little. To clarify the contributions of PDAP, an additional cyclic voltammogram of PDAP-GCE is recorded in the same electrolyte (Fig. 4B). A pair of weak redox peaks is observed at −0.02 and −0.15 V, which is caused by the oxidation and reduction of the PDAP film. Because the peak potentials of PDAP are very close to those of RGO, there is only one pair of broad redox peaks appearing at the PDAP-RGO. It is noted that the oxidation peak current of

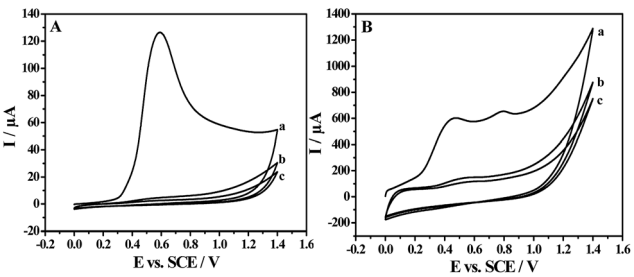

Fig. 1 Cyclic voltammograms of electrochemical polymerization of 2,6-diaminopyridine on bare GCE (A) and RGO modified GCE (B) in 0.1 M NaOH containing 0.1 M NaH_2PO_4 and 20 mM 2,6-diaminopyridine. (a) First cycle; (b) second cycle; and (c) third cycle.

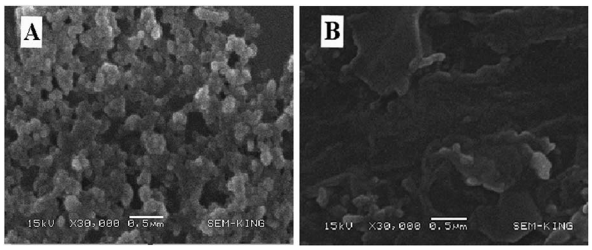

Fig. 2 SEM images of PDAP-GCE (A) and PDAP-RGO (B).

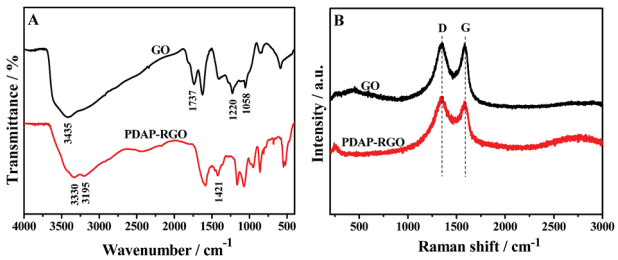

Fig. 3 FT-IR spectra (A) and Raman spectra (B) of GO and PDAP-RGO.

PDAP-RGO (80 μA) is greatly increased compared with that of PDAP-GCE (4 μA), implying the strong electrocatalytic effect of RGO for the growth of PDAP film.

Electrode process and pH dependence of PDAP-RGO

Fig. 5A shows the effect of scan rate (υ) on the cyclic voltammograms of PDAP-RGO. It is evident that both the anodic and the cathodic peak current of PDAP-RGO increase with increasing scan rate from 25 to 250 mV s^{-1}. The linear relationship between the anodic peak current and the scan rate is shown in Fig. 5B, suggesting that the electrode process of PDAP-RGO is surface-controlled. It is found that the straight line deviates slightly from the origin, showing that the electrode process of PDAP-RGO is not an ideal behaviour, which may be attributed to the undesired double-layer charging phenomena.[23,24]

The cyclic voltammograms of PDAP-RGO in 0.1 M PBS of various pH values are shown in Fig. 6A. As can be seen, the anodic peak current decreases significantly with increasing pH value from pH 3.0 to pH 11.0, accompanied by an obvious shift of the

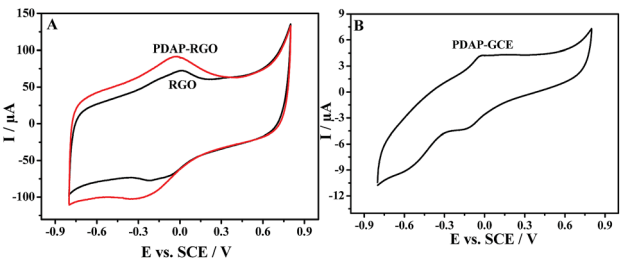

Fig. 4 (A) Cyclic voltammograms of RGO and PDAP-RGO. (B) Cyclic voltammogram of PDAP-GCE. Electrolyte: 0.1 M PBS of pH 7.0. Scan rate: 50 mV s^{-1}.

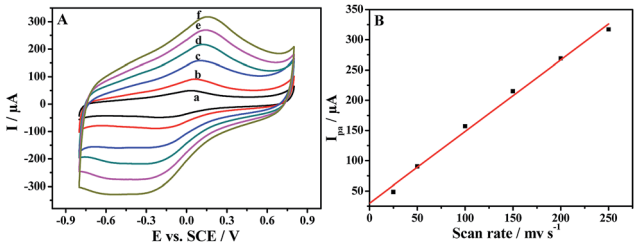

Fig. 5 (A) Cyclic voltammograms of PDAP-RGO in 0.1 M PBS of pH 7.0 at different scan rates: (a) 25; (b) 50; (c) 100; (d) 150; (e) 200 and (f) 250 mV s^{-1}. (B) Linear relationship between anodic peak current and scan rate.

anodic peak potential towards the negative direction (Fig. 6B). This phenomenon implies that protons participate in the redox of PDAP. In other words, protons are de-doped from PDAP film to the electrolyte during the oxidation process, and *vice versa* during the reduction process. It should be emphasized that although the redox activity of PDAP-RGO decreases with increasing pH values, there is still a pair of broad redox peaks at pH 11.0, suggesting that PDAP-RGO still remains good electroactivity till such high pH value. Usually, PDAP loses its electroactivity completely at pH higher than 6.0.[2] In this work, the significantly improved pH dependence of the PDAP-RGO must be attributed to the introduction of RGO. On one hand, the delocalized π-structure of RGO can facilitate the electron transfer at the electrode-solution interface; on the other hand, the subtle residual oxygen-containing functionalities on RGO during the electrochemical reduction of GO, such as –OH and –COOH, can be oxidized and reduced reversibly, and thus they can adjust the acidity in the vicinity of the PDAP-RGO electrode and improve the pH dependence of the PDAP film deposited on RGO.[25–27]

Electrocatalytic reduction of H_2O_2 at PDAP-RGO

Fig. 7A shows the cyclic voltammograms of H_2O_2 of three different concentrations (0, 12.5 and 25 mM) at the PDAP-RGO electrode. It is obvious that the peak at −0.64 V is attributed to the reduction of H_2O_2, since it increases significantly with increasing H_2O_2 concentration. However, it is interesting to find that at individual PDAP (Fig. 7B) and RGO electrode (Fig. 7C), no reduction peak for H_2O_2 is observed.

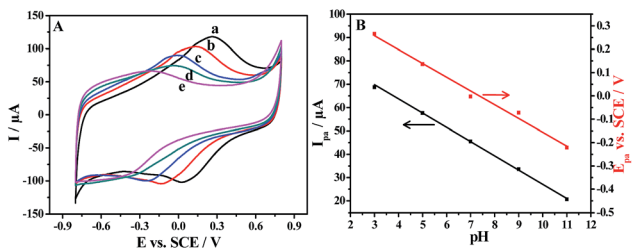

Fig. 6 (A) Cyclic voltammograms of PDAP-RGO in 0.1 M PBS of various pH values at a scan rate of 50 mV s^{-1}: (a) 3.0; (b) 5.0; (c) 7.0; (d) 9.0 and (e) 11.0. (B) Dependencies of anodic peak current and anodic peak potential on pH.

Obviously, the electrocatalytic reduction of H_2O_2 at the PDAP-RGO electrode is caused by the synergistic effect of RGO and PDAP. On one hand, the unique structure of RGO (large delocalized π-electron system) is beneficial to the electron transfer at the electrode-solution interface; on the other hand, there is a large amount of amino and imino groups in PDAP, and these redox-active amino and imino groups in PDAP can function as redox mediators during the electrochemical reduction of H_2O_2, which is similar to the previous reports using Azure A[28] or Prussian blue[29] as the redox mediators. As a result, the synergistic effect of RGO and PDAP leads to the obvious electrocatalytic reduction of H_2O_2 at the PDAP-RGO electrode, as shown in the following equations:

$$PDAP_{oxd}\text{-}RGO + 2ne^- + 2nH^+ \rightarrow PDAP_{red}\text{-}RGO \quad (1)$$

$$nH_2O_2 + PDAP_{red}\text{-}RGO \rightarrow 2nH_2O + PDAP_{oxd}\text{-}RGO \quad (2)$$

$$\text{Total reaction: } H_2O_2 + 2e^- + 2H^+ \rightarrow 2H_2O \quad (3)$$

The calibration curve with only H_2O_2 at the PDAP-RGO electrode is shown in Fig. 8.

Glucose sensing based on PDAP-RGO

Glucose sensing based on the PDAP-RGO electrode is achieved *via* amperometric detection of H_2O_2 at a reduction potential, which is resulted from the oxidation of glucose in the presence of GOD and dissolved oxygen, as shown in the following equations:

$$\beta\text{-glucose} + GOD + O_2 \rightarrow \beta\text{-gluconic acid} + H_2O_2 \quad (4)$$

$$H_2O_2 + 2e^- + 2H^+ \rightarrow 2H_2O \quad (5)$$

Since the current signals are closely related to H_2O_2 concentration, glucose can be accurately quantified by measuring the

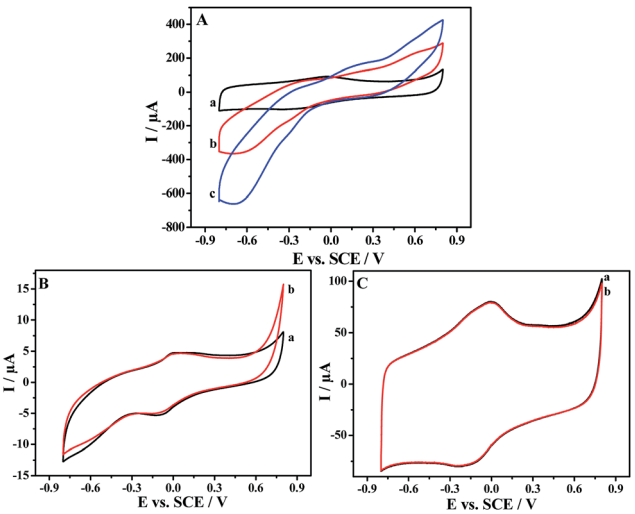

Fig. 7 Cyclic voltammograms of 0 (a), 12.5 (b) and 25 (c) mM H_2O_2 at PDAP-RGO (A), individual PDAP (B) and RGO (C) electrode in 0.1 M N_2-saturated PBS of pH 7.0.

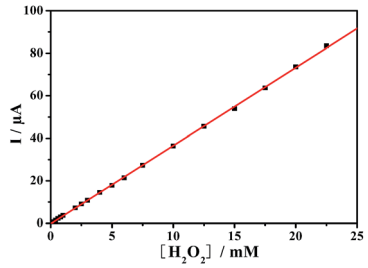

Fig. 8 Linear relationship between current response and H_2O_2 concentration.

produced current responses.[30] Fig. 9A shows typical chronoamperometric responses of the GOD immobilized PDAP-RGO electrode to successive additions of glucose to the stirred air-saturated 0.1 M PBS of pH 7.0 at a negative potential of −0.45 V. The glucose sensor responds quickly to the additions of glucose and reaches to the steady-state current within a short time. As shown in Fig. 9B, the enzyme electrode exhibits a wide linear range for glucose from 0.05 to 6.65 mM with a correlation coefficient of 0.996. The linear regression equation can be expressed as: $I\,(\mu A) = 0.096 + 0.477C\,(mM)\,(n = 13)$. The detection limit is calculated to be 0.142 μM at a signal-to-noise of 3, which is even lower than the non-enzymatic glucose sensors reported previously by our group[11] and other researchers.[31–34]

Apparent Michaelis–Menten constant is an important parameter reflecting the enzyme reaction kinetics, which can be estimated by using Lineweaver–Burk equation.[35] According to the double-reciprocal plot of current *versus* glucose concentration (Fig. 10), the apparent Michaelis–Menten constant is calculated to be 24.73 mM, suggesting a high substrate affinity of the immobilized GOD.

The performance of the proposed biosensor is compared with some of the reported glucose biosensors, as shown in Table 1. The results indicate that the analytical performance of the developed sensor is comparable to those enzymatic and non-enzymatic glucose sensors, even superior to most of them.

Specificity of the detection system

Ascorbic acid (AA) and uric acid (UA) are two common interferents in the detection of glucose. Fig. 11 shows the

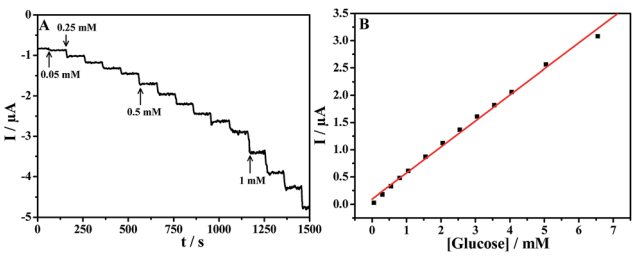

Fig. 9 (A) Chronoamperometric responses of the GOD immobilized PDAP-RGO electrode towards various concentrations of glucose in stirred air-saturated 0.1 M PBS (pH 7.0) at a negative potential of −0.45 V. (B) Linear relationship between current response and glucose concentration.

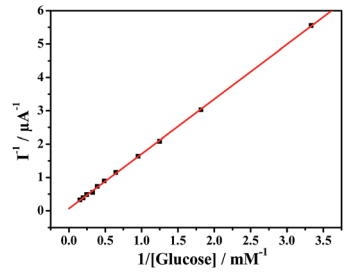

Fig. 10 Double-reciprocal plot of current *versus* glucose concentration.

Table 1 Comparison of the PDAP-RGO based sensor with some enzymatic and non-enzymatic glucose sensors[a]

Materials	Detection limit (μM)	Linear range (mM)	Reference
PDAP/RGO	0.142	0.05–6.55	This work
NiHCF/PANI/G	0.5	0.001–0.765	11
		0.965–13.665	
PdNPs/RGO	0.56	0.025–4.9	17
PtNFs/GO	2.0	0.002–10.3	36
		10.3–20.3	
GOx/Pt/FCNA	0.3	0.5–8	37
PtNPs/SPE	9.3	0.5–3	38

[a] NiHCF/PANI/G, cubic nickel hexacyanoferrate/polyaniline/G; PdNPs/RGO, Pd nanoparticles/RGO; PtNFs/GO, Pt nanoflowers/GO; GOx/Pt/FCNA, glucose oxidase/Pt/flower-like carbon nanosheet aggregation; PtNPs/SPE, Pt nanoparticles/screen printed electrode.

amperometric responses to successive additions of 5 mM glucose, 0.1 mM AA and 0.3 mM UA recorded at the PDAP-RGO based sensor at −0.45 V in 0.1 M PBS of pH 7.0. It is shown that proposed sensor exhibits excellent selectivity to glucose in the presence of AA and UA.

Reproducibility and stability

The intra- and interassay reproducibility of the PDAP-RGO based glucose sensor were tested. The intraassay reproducibility was examined by continuous determination of 1 mM glucose with the same GOD immobilized electrode for five times, and the relative standard deviation (RSD) is calculated to

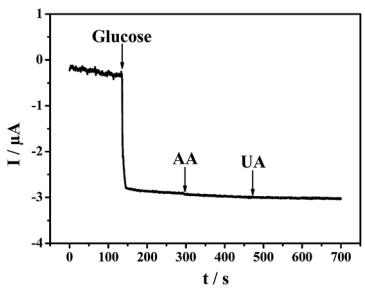

Fig. 11 Amperometric responses of the PDAP-RGO based sensor to successive additions of 5 mM glucose, 0.1 mM AA and 0.3 mM UA at an applied potential of −0.45 V in 0.1 M PBS (pH 7.0).

Table 2 Amperometric determination of glucose in three human blood serum samples

Serum sample	Clinical analyzer (mM)	The proposed sensor (mM)	RSD ($n = 5$)
1	4.58	4.54	2.64%
2	4.97	5.02	7.58%
3	5.33	5.29	4.95%

be as small as 2.87%. Meanwhile, the interassay reproducibility was also estimated by measuring 1 mM glucose with five independent PDAP-RGO electrodes prepared *via* the same procedure, and a RSD of 3.28% is obtained. The small RSDs in intra- and interassay suggest that the GOD immobilized PDAP-RGO electrode has good preparation and determination reproducibility. In addition, the stability of the proposed PADP-RGO based glucose sensor was also assessed. The sensor was stored at 4 °C in 0.1 M PBS of pH 7.0, and the current responses of 1 mM glucose were recorded periodically. It is found that the current signal changes little during the first week, and it still remains at about 94% of the initial response after two weeks of storage. The results indicate that the as-prepared glucose sensor has satisfactory stability.

Analysis of real samples

Analysis of real samples with the proposed PDAP-RGO based sensor was performed by determining glucose concentration in three human blood serum samples. The results are listed in Table 2, and the analysis results from a standard clinical analyzer are also provided for comparison. As can be seen, the data obtained from the proposed sensor are similar to those measured by the clinical analyzer, indicating that the sensor possesses biosensing possibility for real samples.

Conclusions

In summary, RGO plays a decisive role in the electrochemical polymerization of 2,6-diaminopyridine, and the obtained PDAP film has an improved pH dependence compared with that deposited directly on GCE. More important, the formed PADP-RGO has significant catalytic activity towards the electrochemical reduction of H_2O_2 due to the synergistic effect of RGO and PDAP, and thus a sensitive glucose sensing platform is constructed *via* immobilizing GOD to the PDAP-RGO electrode. The prepared glucose sensor displays excellent performances for glucose sensing, opening a new avenue for the construction of biocatalysis and biosensing platform *via* combining the advantages of conducting polymers and RGO based carbon nanomaterials.

Acknowledgements

The authors are grateful to the National Natural Science Foundation of China (21275023, 21173183), Natural Science Foundation of Jiangsu Province (BK2012593), Jiangsu Key Laboratory

of Advanced Catalytic Materials and Technology (BM2012110), Jiangsu Key Laboratory of Fine Petrochemical Engineering (KF1305) and Priority Academic Program Development of Jiangsu Higher Education Institutions (PAPD).

References

1 M. M. Maricq, J. S. Waugh, A. G. MacDiarmid, H. Shirakawa and A. J. Heeger, *J. Am. Chem. Soc.*, 1978, **100**, 7729.
2 Z. Liu, Q. X. Liu, X. Dai, C. Shen-Tu, C. Yao and Y. Kong, *ECS Electrochem. Lett.*, 2013, **2**, G1.
3 S. R. Cao, R. Yuan, Y. Q. Chai, L. Y. Zhang, X. L. Li and R. Chai, *J. Electrochem. Soc.*, 2006, **153**, H223.
4 S. R. Cao, R. Yuan, Y. Q. Chai, L. Y. Zhang, X. L. Li and F. X. Gao, *Bioprocess Biosyst. Eng.*, 2007, **30**, 71.
5 S. P. Luo, Q. X. Liu, Z. Liu, A. J. Xie, Y. Kong and X. Dai, *Chin. Chem. Lett.*, 2012, **23**, 1311.
6 K. S. Novoselov, A. K. Geim, S. V. Morozov, D. Jiang, Y. Zhang, S. V. Dubonos, I. V. Grigorieva and A. A. Firsov, *Science*, 2004, **306**, 666.
7 H. Kim, Y. Miura and C. W. Macosko, *Chem. Mater.*, 2010, **22**, 3441.
8 M. A. Rafiee, J. Rafiee, I. Srivastava, Z. Wang, H. Song, Z. Z. Yu and N. Koratkar, *Small*, 2010, **6**, 179.
9 W. L. Chen and S. L. Mu, *Electrochim. Acta*, 2011, **56**, 2284.
10 S. L. Mu, *Electrochim. Acta*, 2011, **56**, 3764.
11 Y. Kong, Y. Sha, Y. X. Tao, Y. Qin, H. G. Xue and M. H. Lu, *J. Electrochem. Soc.*, 2014, **161**, B269.
12 Y. Kong, T. Zhou, Y. Qin, Y. X. Tao and Y. Wei, *J. Electrochem. Soc.*, 2014, **161**, H573.
13 J. Qiu, L. Shi, R. Liang, G. Wang and X. Xia, *Chem.–Eur. J.*, 2012, **18**, 7950.
14 S. Alwarappan, C. Liu, A. Kumar and C. Z. Li, *J. Phys. Chem. C*, 2010, **114**, 12920.
15 A. Wisitsoraat, S. Pakapongpan, C. Sriprachuabwong, D. Phokharatkul, P. Sritongkham, T. Lomas and A. Tuantranont, *J. Electroanal. Chem.*, 2013, **704**, 208.
16 D. C. Marcano, D. V. Kosynkin, J. M. Berlin, A. Sinitskii, Z. Z. Sun, A. Slesarev, L. B. Alemany, W. Lu and J. M. Tour, *ACS Nano*, 2010, **4**, 4806.
17 Y. Qin, Y. Kong, Y. Y. Xu, F. Q. Chu, Y. X. Tao and S. Li, *J. Mater. Chem.*, 2012, **22**, 24821.
18 M. Zhou, Y. L. Wang, Y. M. Zhai, J. F. Zhai, W. Ren, F. Wang and S. J. Dong, *Chem.–Eur. J.*, 2009, **15**, 6116.
19 W. P. Zhang, J. Zhang, T. Bao, W. Zhou, J. W. Meng and Z. L. Chen, *Anal. Chem.*, 2013, **85**, 6846.
20 D. R. Dreyer, S. Park, C. W. Bielawski and R. S. Ruoff, *Chem. Soc. Rev.*, 2010, **39**, 228.
21 Z. H. Liu, H. H. Zhou, Z. Y. Huang, W. Y. Wang, F. Y. Zeng and Y. F. Kuang, *J. Mater. Chem. A*, 2013, **1**, 3454.
22 Q. L. Hao, X. F. Xia, W. Lei, W. J. Wang and J. S. Qiu, *Carbon*, 2015, **81**, 552.
23 S. Shreepathi and R. Holze, *Chem. Mater.*, 2005, **17**, 4078.
24 S. Bilal and R. Holze, *J. Electroanal. Chem.*, 2006, **592**, 1.
25 S. L. Mu, *Synth. Met.*, 2004, **143**, 259.
26 C. X. Chen, C. Sun and Y. H. Gao, *Electrochim. Acta*, 2008, **53**, 3021.
27 C. X. Chen, C. Sun and Y. H. Gao, *Electrochem. Commun.*, 2009, **11**, 450.
28 C. Priya, G. Sivasankari and S. S. Narayanan, *Colloids Surf., B*, 2012, **97**, 90.
29 X. Zhong, R. Yuan and Y. Q. Chai, *Sens. Actuators, B*, 2012, **162**, 334.
30 S. Cosnier, C. Gondran, A. Senillou, M. Gratzel and N. Vlachopoulos, *Electroanalysis*, 1997, **9**, 1387.
31 J. Chen, W. D. Zhang and J. S. Ye, *Electrochem. Commun.*, 2008, **10**, 1268.
32 M. Shamsipur, M. Najafi and M. R. M. Hosseini, *Bioelectrochemistry*, 2010, **77**, 120.
33 Y. J. Lee and J. Y. Park, *Sens. Actuators, B*, 2011, **155**, 134.
34 X. H. Kang, Z. B. Mai, X. Y. Zou, P. X. Cai and J. Y. Mo, *Anal. Biochem.*, 2007, **363**, 143.
35 R. A. Kamin and G. S. Wilson, *Anal. Chem.*, 1980, **52**, 1198.
36 G. H. Wu, X. H. Song, Y. F. Wu, X. M. Chen, F. Luo and X. Chen, *Tanala*, 2013, **105**, 379.
37 S. Tang, X. Z. Wang, J. P. Lei, Z. Hu, S. Y. Deng and H. X. Ju, *Biosens. Bioelectron.*, 2010, **26**, 432.
38 J. Yang, Y. G. Nam, S. K. Lee, C. S. Kim, Y. M. Koo, W. J. Chang and S. Gunasekaran, *Sens. Actuators, B*, 2014, **203**, 44.